Extremum-Seeking-Based Receding-Horizon Optimal Control of Plasma Current Profile in the DIII-D Tokamak ⋆

Y. Ou, C. Xu, E. Schuster *
T.C. Luce, J.R. Ferron, M.L. Walker and D.A. Humphreys **

* *Mechanical Engineering & Mechanics, Lehigh University, Bethlehem, USA*
** *General Atomics, San Diego, USA*

Abstract:
A key goal in the control of a magnetic fusion reactor is to maintain current profiles that are compatible with a high fraction of self-generated non-inductive current as well as with magnetohydrodynamic (MHD) stability at high plasma pressure. This enables high fusion gain and noninductive sustainment of plasma current for steady-state operation. The approach taken toward establishing such plasma current profiles at the DIII-D tokamak is to create the desired profile during the plasma current ramp-up and early flattop phases. The evolution in time of the current profile is related to the evolution of the poloidal flux, which is modeled in normalized cylindrical coordinates using a nonlinear partial differential equation (PDE) usually referred to as the magnetic diffusion equation. We propose, and test in simulations, an extremum-seeking-based, receding-horizon, diffusivity-interior-boundary control scheme designed to match as close as possible a desired current profile within a prespecified time interval.

1. INTRODUCTION

Fusion energy, the power source of the sun, represents a virtually unlimited source of energy for humanity. In a fusion reaction, two light atoms such as hydrogen fuse to form a heavier atom and release energy. Since nuclei carry positive charges, they normally repel one another when trying to fuse. To overcome the Coulomb barrier, the kinetic energy of the nuclei must be increased by heating. The fusion process requires extremely high temperatures (50 to 200 million Kelvin), at which the hydrogen gas ionizes and becomes a plasma, which conducts electricity and interacts with magnetic fields.

One of the most promising approaches to fusion is the magnetic confinement concept. Strong magnetic fields act like a magnetic bottle to hold the ionized (charged) nuclei together and away from the vessel wall as they are heated to fusion temperatures. A Russian design in the shape of a torus, called tokamak, has proved particularly well suited for containing a fusion plasma. A more in-depth introduction to fusion can be found in Pironti and Walker [2005], Walker et al. [2006], Schuster and Ariola [2006], in which considerable effort was made to describe the problems of tokamak plasma control at a level that is accessible to engineers, mathematicians, and non-plasma physicists.

In a tokamak, the magnetic field lines twist their way around the torus to form a helical structure. It is possible to use the poloidal component of the helicoidal magnetic lines to define nested toroidal surfaces corresponding to constant values of the poloidal magnetic flux. As it is illustrated in Fig. 1, the poloidal flux ψ at a point P in the (r,z) cross section of the plasma (i.e., poloidal cross section) is the total flux through the surface S bounded by the toroidal ring passing through P, i.e., $\psi = \int B_{pol} dS$. The dynamics of the poloidal flux ψ is governed by a nonlinear parabolic PDE.

Setting up a suitable current profile, or equivalently, a suitable poloidal flux profile, has been demonstrated to be a key condition for improved confinement and possible steady-state operation (Murakami et al. [2006]). Recent experiments at different devices around the world (DIII-D: Ferron et al. [2006], JET: Moreau et al. [2003], Laborde et al. [2005], JT-60U: Suzuki et al. [2005], Tore Supra: Wijnands et al. [1997]) have demonstrated significant progress in achieving profile control. Experiments at DIII-D focus on creating the desired current profile during the plasma current ramp-up and early flattop phases with the aim of maintaining this target profile during the subsequent phases of the discharge. Since the actuators are constrained, a perfect matching of the desirable target profile may not be physically possible for all arbitrary initial conditions. In practice, the objective is to achieve the best possible approximate matching in a short time window $[T_1, T_2]$ during the early flattop phase of the total plasma current pulse, as shown in Fig. 2. Thus, such a matching problem can be treated as an optimal control problem for a nonlinear PDE system. In this paper, a closed-loop, extremum-seeking-based, receding-horizon, optimal controller is proposed as solution to this problem.

The paper is organized as follows. In Section 2, an infinite-dimensional dynamic model for the poloidal flux ψ is introduced. Section 3 describes the control objectives during the different phases of the tokamak discharge, and states the control problem. In Section 4, a closed-loop, extremum-seeking-based, receding-horizon controller that makes use of diffusivity, interior, and boundary actuation is proposed. A simulation study showing the effectiveness of the proposed closed-loop controller is presented in Section 5. Finally, conclusions and identified future work are stated in Section 6.

⋆ This work was supported in part by a grant from the Commonwealth of Pennsylvania, Department of Community and Economic Development, through the Pennsylvania Infrastructure Technology Alliance (PITA), the NSF CAREER award program (ECCS-0645086), and DoE contract number DE-FC02-04ER54698. Corresponding author: yoo205@lehigh.edu

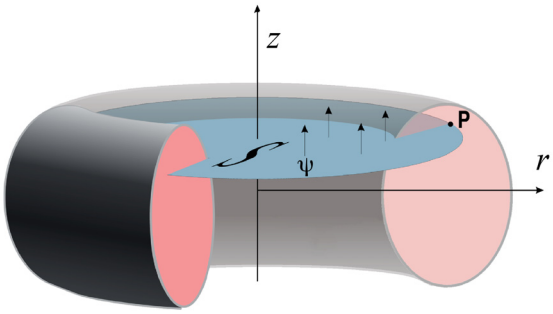

Fig. 1. Poloidal flux in a tokamak.

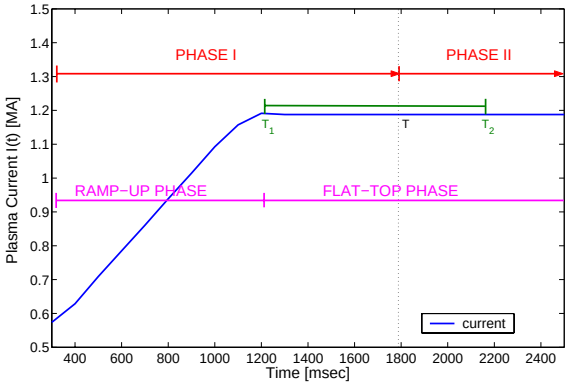

Fig. 2. Plasma current evolution.

2. CURRENT PROFILE EVOLUTION MODEL

We let ρ be an arbitrary coordinate indexing the surfaces of constant magnetic flux. Any quantity constant on each magnetic surface could be chosen as the variable ρ. We choose the mean geometric radius of the magnetic surface as the variable ρ, i.e., $\pi B_{\phi,o}\rho^2 = \Phi$, where Φ is the toroidal magnetic flux. The evolution of the poloidal flux in normalized cylindrical coordinates is given by the magnetic diffusion equation (Hinton and Hazeltine [1976]),

$$\frac{\partial \psi}{\partial t} = \frac{\eta(T_e)}{\mu_o \rho_b^2 \hat{F}^2 \hat{\rho}} \frac{\partial}{\partial \hat{\rho}} \left(\hat{\rho} \hat{F} \hat{G} \hat{H} \frac{\partial \psi}{\partial \hat{\rho}} \right) - R_o \hat{H} \eta(T_e) \frac{<\bar{j}_{NI} \cdot \bar{B}>}{B_{\phi,o}}, \quad (1)$$

where all the parameters are defined in Table 1.

The model (1) is based on the following assumptions: a) The vacuum toroidal field is constant in time (usually true in practice), b) The map of $\hat{\rho}$ in real space is constant in time (true if plasma boundary control regulates to a constant reference). The boundary conditions of (1) are given by

$$\left.\frac{\partial \psi}{\partial \hat{\rho}}\right|_{\hat{\rho}=0} = 0, \quad \left.\frac{\partial \psi}{\partial \hat{\rho}}\right|_{\hat{\rho}=1} = \frac{\mu_o}{2\pi} \frac{R_o}{\hat{G}|_{\hat{\rho}=1} \hat{H}|_{\hat{\rho}=1}} I(t), \quad (2)$$

where $I(t)$ denotes the total plasma current.

The current density that flows toroidally around the tokamak, $< \bar{j} \cdot \bar{B}/B_{\phi,o} >$, and whose profile must be controlled, is related to spatial derivative of the poloidal magnetic flux,

$$\frac{<\bar{j} \cdot \bar{B}>}{B_{\phi,o}} = \frac{1}{\mu_o \rho_b^2 \hat{F}^2 \hat{H} \hat{\rho}} \frac{\partial}{\partial \hat{\rho}} \left(\hat{\rho} \hat{F} \hat{G} \hat{H} \frac{1}{R_0} \frac{\partial \psi}{\partial \hat{\rho}} \right). \quad (3)$$

During "Phase I" (see Fig. 2), mainly governed by the plasma current ramp-up phase, the plasma current is mostly driven by induction. In this case, it is possible to decouple the equation for the evolution of the poloidal flux from the evolution equations for the temperature $T_e(\hat{\rho},t)$ and the density $n_e(\hat{\rho},t)$. Highly simplified models for the density, temperature, and non-inductive toroidal current density are chosen for this phase (Ou et al. [2006]). The profiles are assumed to remain fixed. The responses to the actuators are simply scalar multiples of the reference profiles. These reference profiles are taken from a DIII-D tokamak discharge.

The density n is independently controlled and written as

$$n(\hat{\rho},t) = n^{profile}(\hat{\rho}) u_n(t), \quad (4)$$

where $n^{profile}$ is given in Fig. 4. The average density is defined as $\bar{n}(t) = \int_0^1 n(\hat{\rho},t) d\hat{\rho}$.

The temperature T_e is proportional to $\frac{I(t)\sqrt{P_{tot}}}{\bar{n}(t)}$ and written as

$$T_e(\hat{\rho},t) = k_{Te} T_e^{profile}(\hat{\rho}) \frac{I(t)\sqrt{P_{tot}}}{\bar{n}(t)}, \quad (5)$$

where $k_{Te} = 1.7295 \cdot 10^{10}$ $(m^{-3}A^{-1}W^{-1/2})$, $T_e^{profile}$ is given in Fig. 4, and P_{tot} is the total power deposited by the non-inductive current sources (Electron Cyclotron Heating (ECH), Neutral Beam Heating (NBH), etc.).

The non-inductive toroidal current density $\frac{<\bar{j}_{NI} \cdot \bar{B}>}{B_{\phi,o}}$ is written as

$$\frac{<\bar{j}_{NI} \cdot \bar{B}>}{B_{\phi,o}} = k_{NIpar} j_{NIpar}^{profile}(\hat{\rho}) \frac{I(t)^{1/2} P_{tot}(t)^{5/4}}{\bar{n}(t)^{3/2}}, \quad (6)$$

where $j_{NIpar}^{profile}$ is given in Fig. 4, and $k_{NIpar} = 1.2139 \cdot 10^{18}$ $(m^{-9/2}A^{-1/2}W^{-5/4})$.

The resistivity η scales with the temperature T_e as

$$\eta(\hat{\rho},t) = \frac{k_{eff} Z_{eff}}{T_e^{3/2}(\hat{\rho},t)}, \quad (7)$$

where $Z_{eff} = 1.5$, and $k_{eff} = 4.2702 \cdot 10^{-8}$ $(\Omega m (kev)^{3/2})$.

We consider $\bar{n}(t)$, $I(t)$, and $P_{tot}(t)$ as the physical actuators of the system. Therefore, we can modify the poloidal flux profile dynamics via the non-inductive toroidal current density $\frac{<\bar{j}_{NI} \cdot \bar{B}>}{B_{\phi,o}}$ (interior control), the total plasma current $I(t)$ (boundary control), and the plasma resistivity η (diffusivity control).

3. CONTROL PROBLEM DESCRIPTION

The control objective, as well as the dynamic models for current profile evolution, depend on the phases of the discharge (Fig. 2). During "Phase I" the control goal is to drive the current profile from any arbitrary initial condition to a prescribed target or desirable profile at some time $T \in (T_1, T_2)$ (here $T_1 = 1.2s$ and $T_2 = 2.4s$) in the flat-top phase of the total current $I(t)$ evolution. However, since the available actuators during "Phase I" differ from those used during "Phase II," and are constrained, the prescribed target profile is not an equilibrium profile during "Phase I". During "Phase II" the control goal is to regulate the current profile using as little control effort as possible because the actuators are not only limited in power but also in energy. For this reason, the goal during "Phase I" is to set up an initial profile for "Phase II" as close as possible to its desirable profile.

In this paper, we focus on "Phase I." An optimal control problem must be solved, where control laws $I(t)$, $P_{tot}(t)$, and $\bar{n}(t)$ are sought to minimize the cost functional

Table 1. Description of parameters

Parameters	Description
ψ	poloidal flux
$\eta(T_e)$	plasma resistivity
T_e	electron temperature
n	plasma density
$\mu_o = 4\pi \times 10^{-7}$ $(\frac{\mathrm{H}}{\mathrm{m}})$	vacuum permeability
$\rho_b = 0.79$ (m)	radius of last closed flux surface
Φ_b	toroidal flux for the last closed flux surface
$B_{\phi,o} = 1.85\ T$	reference magnetic field at R_o
$R_o = 1.668$ (m)	reference point for $B_{\phi,o}$
	(e.g., geometric center of plasma R_{geo})
$\hat{\rho}$	ρ/ρ_b
$\hat{F}, \hat{G}, \hat{H}$	Geometric factors (functions of $\hat{\rho}$ (Fig. 3))
j_{NI}	non-inductive source of current density
	(neutral beam, electron cyclotron, etc.)
$<>$	flux-surface average
j	current density
E	electric field
$\sigma(T) = 1/\eta(T)$	plasma conductivity
I	total plasma current
P_{tot}	total power of non-inductive current drives
$\bar{n}$	spatially averaged density

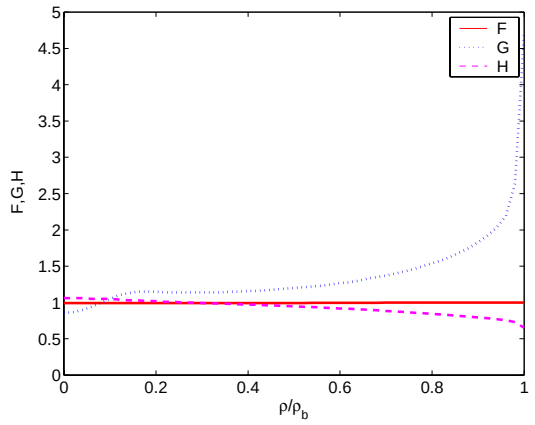

Fig. 3. Geometric factors F, G, and H.

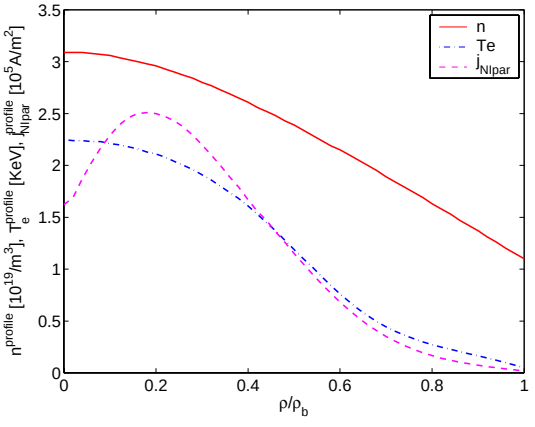

Fig. 4. Density ($n^{profile}$), temperature ($T_e^{profile}$), and non-inductive toroidal current density ($j_{NIpar}^{profile}(\hat{\rho})$) profiles.

$$J = \sqrt{\frac{1}{M}\min(J^*(t_j))}, \tag{8}$$

where t_j are discrete points in time equally spaced within the interval $[T_1, T_2]$, e.g., $t(j) = 1.2s, 1.3s, 1.4s, \ldots, 2.4s$ for $j = 1, 2, 3, \ldots, 13$, and $J^*(t_j)$ is given by

$$J^*(t_j) = \sum_{i=1}^{M} (\iota(\hat{\rho}_i, t_j) - \iota^{des}(\hat{\rho}_i))^2, \tag{9}$$

where M is the number of discrete points in space within the interval $[0,1]$ for the normalized radius. Here ι is the rotational transform, the inverse of the safety factor q and a measure of the helicity of the magnetic field lines. This figure of merit is proportional to the current density and is defined as

$$\iota(\rho,t) = \frac{2\pi}{q(\rho,t)} = \frac{\partial\psi(\rho,t)}{\partial\Phi} = \frac{\partial\psi}{\partial\hat{\rho}}\frac{1}{B_{\phi,o}\rho_b^2\hat{\rho}}, \tag{10}$$

where $B_{\phi,o}$ and ρ_b are defined in Table 1.

"Phase I" can be roughly divided into two phases, the ramp-up phase and the flattop phase. During the ramp-up phase, the three actuators $I(t)$, $\bar{n}(t)$ and $P_{tot}(t)$ are available, whereas during the flattop phase we can only vary $P_{tot}(t)$ keeping $I(t)$ and $\bar{n}(t)$ fixed at some predetermined values. In addition to these specific constraints during the flattop phase, the absolute values, and sometimes the derivatives in time, of the control variables must be within some specific limits during the whole "Phase I". The physical ranges for $I(t)$, $\bar{n}(t)$ and $P_{tot}(t)$ are given by

$$0 \le I(t) \le I_{max}, \quad \left|\frac{dI(t)}{dt}\right| \le dI_{max}, \tag{11}$$

$$I(\mathrm{MA}) \le \frac{\bar{n}(t)}{10^{19}} \le 5I(\mathrm{MA}), \tag{12}$$

$$0 \le P_{tot}(t) \le P_{max}. \tag{13}$$

To accurately reproduce experimental discharges, we must add constraints for $I(t)$ and $\bar{n}(t)$ at the initial time of "Phase I", i.e., $I(t = 0s) = I_0$, $\bar{n}(t = 0s) = \bar{n}_0$. In addition, a value of the total current $I(t)$ is prescribed for the flattop phase, i.e., $I(t \ge T_1) = I_{target}$, where T_1 marks the end of the ramp-up phase and the start of the flattop phase (Fig. 2).

In summary, the optimal control problem (8) must be solved taking into account that (i) during the ramp-up phase ($0 \le t \le T_1$) we can manipulate the three actuators by obeying the physical constraints (11)–(13) and their initial conditions, (ii) during the flattop phase $I(t)$ must be equal to I_{target} and $\bar{n}(t)$ must be equal to $\bar{n}(T_1)$. We seek $I(t)$, $\bar{n}(t)$ and $P_{tot}(t)$ for $t \in [0,T]$ that makes $\iota(\hat{\rho},T)$ as close as possible to the prescribed target profile $\iota^{des}(\hat{\rho})$ at some time $T \in [T_1, T_2]$.

4. CLOSED LOOP OPTIMAL CONTROL

In this section, we present a closed-loop, receding-horizon, optimal controller based on an extremum-seeking optimization framework.

4.1 Receding Horizon Control

A controller belonging to the Receding Horizon Control family solves an optimization problem at each sampling time t_i. In this particular case, given $\psi(\hat{\rho},t_i)$, the PDE model (1)-(2) is used to predict the the output $\psi(\hat{\rho},t)$, for $t \ge t_i$, which can be in turn employed to compute $\iota(\hat{\rho},T)$ using (10). By minimizing the cost function (8), the future trajectories for the control input $u(t)$, for $t \ge t_i$, are obtained. When the optimization is completed, the calculated control input $u(t)$, for $t_{i+1} \le t \le t_{i+2}$, is implemented on the actual system, while the rest of the computed control inputs are discarded. This is because the

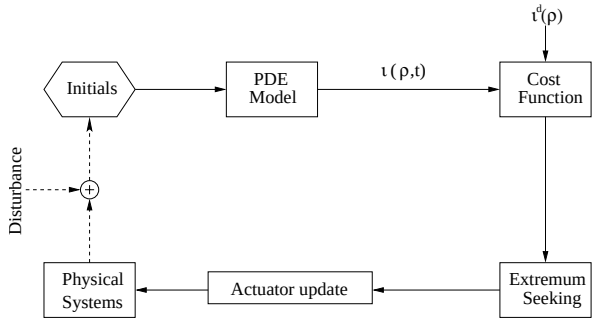

Fig. 5. Closed-loop control block diagram.

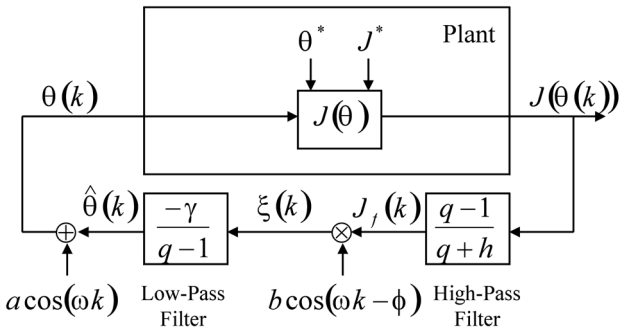

Fig. 6. Extremum seeking control scheme.

output $\psi(\hat{\rho},t_{i+1})$ is measured at the sampling instant t_{i+1}, and used as the initial poloidal flux profile in a new optimization problem that provides the control input for for $t_{i+2} \le t \le t_{i+3}$. Initially, approximate actuator trajectories $u(t)$, for $t \ge t_0 = 0$, are calculated off-line using the extremum seeking algorithm and considering an initial poloidal flux profile that may be different from the measured poloidal flux profile at $t_0 = 0$. However, only $u(t)$, for $t_0 = 0 \le t \le t_1$, will be implemented in the system without feedback correction. As illustrated in Fig. 5, the measure of the poloidal flux profile ψ at each sampling time t_i as the response to previous control inputs $u(t)$, for $t < t_i$, represents a closed-loop strategy.

4.2 Extremum Seeking Optimization

An extremum seeking algorithm has been implemented for the solution of the optimal control problem (8) at each sampling time t_i, for $i = 0,\ldots,N-1$. Extremum seeking (Ariyur and Krstic [2003]) is applicable in situations where there is a nonlinearity in the control problem, and the nonlinearity has a local minimum or a maximum. The parameter space can be multidimensional. Here, we use extremum seeking for iterative optimization of the parameters θ (shown in Fig. 6) to make the quadratic error between $\iota(\hat{\rho},T)$ and the prescribed target profile $\iota^{des}(\hat{\rho})$ as small as possible at some time $T \in [T_1,T_2]$, i.e., to minimize J in (8).

We change parameters θ after each plasma "discharge." Thus, we employ the discrete time variant of extremum seeking (J. Choi and Lee [2002]). The implementation is depicted in Fig. 6, where q denotes the variable of the Z-transform. The high-pass filter is designed as $0 < h < 1$, and the modulation frequency ω is selected such that $\omega = \alpha\pi$, $0 < |\alpha| < 1$, and α is rational. The static nonlinear block $J(\theta)$ corresponds to one "discharge" of the system. The objective is to minimize J. If J has a global minimum, its value is denoted by J^* and its argument by θ^*. Given the simulated profile $\iota(\hat{\rho},t)$ for $t \in [t_i,T_2]$ at iteration k, the output of the nonlinear static map, $J(k) = J(\theta(k))$, is obtained by evaluating (8) and used to compute $\theta(k+1)$ according to the extremum seeking procedure in the Fig. 6, or written equivalently as

$$J_f(k) = -hJ_f(k-1) + J(k) - J(k-1), \tag{14}$$

$$\xi(k) = J_f(k)b\cos(\omega k - \phi), \tag{15}$$

$$\hat{\theta}(k+1) = \hat{\theta}(k) - \gamma\xi(k), \tag{16}$$

$$\theta(k+1) = \hat{\theta}(k+1) + a\cos(\omega(k+1)), . \tag{17}$$

In a simulation environment, we understand by "discharge" the integration of the PDE equation (1)–(2) in the interval $[t_i,T_2]$. In each iteration of the extremum seeking procedure, $\theta(k)$ is used to compute the time evolution of the three physical actuators $I(t)$, $\overline{n}(t)$ and $P_{tot}(t)$ in this time interval. At each sampling time t_i, the vector parameter θ has 10 components given by

$$\theta = [I(t_i^{I1}), I(t_i^{I2}), P_{tot}(t_i), P_{tot}(t_i^{P1}), P_{tot}(t_i^{P2}), P_{tot}(T_1), \overline{n}(t_i^{n1}), \overline{n}(t_i^{n2}), \overline{n}(t_i^{n3}), \overline{n}(T_1)], \tag{18}$$

where $t_i < t_i^{I1}, t_i^{I2}, t_i^{P1}, t_i^{P2}, t_i^{n1}, t_i^{n2}, t_i^{n3} < T_1$. By taking into account that $I(t_i)$ is fixed by the outcome of the optimization at $t = t_{i-1}$, or by the initial condition ($I(0s) = I_0$), and $I(T_1) = I_{target}$, and using polynomial curve fitting for the points $I(t_i), I(t_i^{I1}), I(t_i^{I2}), I(T_1)$, we can reconstruct the profile for $I(t)$ for $t \in [t_i,T_1]$. In addition, we make $I(t) = I_{target}$ for $t \in (T_1,T_2]$. Following similar procedure, we can reconstruct the law for $P_{tot}(t)$. In this case we have the freedom to modify both $P_{tot}(t_i)$ and $P_{tot}(T_1)$. By considering that $\overline{n}(t_i)$ is fixed by the outcome of the optimization at t_{i-1} or by the initial condition ($\overline{n}(0s) = \overline{n}_0$), and using polynomial curve fitting, we can define the law for $\overline{n}(t)$ for $t \in [t_i,T_2]$ ($\overline{n}(t) = \overline{n}(T_1)$ for $t \in (T_1,T_2]$). The reconstructed control laws are in turn fed into the PDE system (1)–(2). Given ψ_{ini}, the PDE equation is integrated to obtain $\psi(\hat{\rho},t)$, and finally $\iota(\hat{\rho},t)$, which are necessary to evaluate the cost function, $J(k) = J(\theta(k))$, in (8).

4.3 Receding Horizon Extremum Seeking Algorithm

The combination of the receding horizon control framework and the extremum seeking optimization technique can be summarized in the following algorithm:

At each sampling time select the tolerance $\varepsilon > 0$ and the maximum number of iterations for the extremum seeking optimal control algorithm, load the desirable $\iota^{des}(\hat{\rho})$ profile data and perform the following steps:

1) *Define $t_i = t_0$. Consider an off-line actuator trajectories $u(t)$, for $t \ge t_i = t_0$.*
2) *Implement the actuator trajectories $u(t)$ on the actual system for $[t_i, t_i + \Delta t]$, measure the output of the actual system $\psi(\hat{\rho},t_i)$. Reset the iteration number k.*
3) *Using the measured poloidal flux at time t_i and the actuator trajectories $u(t)$ for $t \ge t_i$, compute the predicted $\iota(\hat{\rho},t)$ from the output sequence $\psi(\hat{\rho},t)$, for $t \ge t_i$, obtained from the PDE model. Increment k.*
4) *Compute the cost function (8). If it is less than ε or the maximum number of iterations is reached, go to step 6).*
5) *Adjust the parameters $\theta(k)$ (i.e, $u(t)$) using the extremum seeking algorithm, and go to step 3).*
6) *Make $t_i = t_i + \Delta t$, and go to step 2).*

5. SIMULATION RESULTS

We present three simulations cases. In the first case, the extremum-seeking algorithm is used in open-loop to solve the optimization problem (8) for a nominal initial profile. The limitations of the open-loop controller to cope with disturbances in the initial profile is manifested in the second case, where a disturbed initial profile is considered. Finally, in the third case, the performance of the closed-loop controller is analyzed when the same disturbed initial profile is considered.

In these simulations, we consider the time interval $[0, T_2 = 2.4s]$. The current $I(t)$ is reconstructed in $[0, T_1 = 1.2s]$ using polynomial interpolation to fit the discrete points $I(t=0) = 0.709229$ MA, θ_1, θ_2, $I(t = T_1 = 1.2s) = 1.18774$ MA. In addition, $I(t) = 1.18774$ MA in $[T_1, T_2]$. The parameters $I_{max} = 1.19141$ MA and $dI_{max} = 2\,\mathrm{MA/s}$ are used in (11) to evaluate the constraints for $I(t)$.

The total power $P_{tot}(t)$ is reconstructed using polynomial interpolation to fit the discrete points θ_3, θ_4, θ_5, $\theta_6 = P_{tot}(t = T_1 = 1.2s)$. For $t > T_1 = 1.2s$, $P_{tot}(t) = P_{tot}(T_1)$. The constraint for $P_{tot}(t)$ is evaluated from (13) using $P_{max} = 20$ MW.

The average density $\overline{n}(t)$ is obtained by similar procedure, given the discrete points $\overline{n}(t=0) = 2 \times 10^{10} m^{-3}$, θ_7, θ_8, θ_9, $\overline{n}(t = T_1 = 1.2s) = \theta_{10}$. For $t > T_1 = 1.2s$, $\overline{n}(t) = \overline{n}(T_1)$. The constraints for $\overline{n}(t)$ are given by (12).

The initial values for θ are arbitrarily chosen as

$$\begin{aligned}\theta_{ini} = [&0.938721\,MA, 1.15723\,MA, 1.15723\,MW,\\ &0.860596\,MW, 1.09253\,MW, 1.09253 \times 2\,MW,\\ &1 \times 10^{19} m^{-3}, 2 \times 10^{19} m^{-3}, 3 \times 10^{19} m^{-3}, 4 \times 10^{19} m^{-3}],\end{aligned}$$

with $i = 0$, $t_0 = 0s$, $t_0^{I1} = 0.4s$, $t_0^{I2} = 0.8s$, $t_0^{P1} = 0.4s$, $t_0^{P2} = 0.8s$, $t_0^{n1} = 0.3s$, $t_0^{n2} = 0.6s$, $t_0^{n3} = 0.9s$. Note that θ_1, θ_2, θ_3, θ_4, θ_5, θ_7, θ_8, θ_9 are redefined at each sampling time t_i (see (18)).

5.1 Open-loop control

The nominal initial poloidal flux ψ considered in this simulation case is shown in Fig. 7(a). The target or desirable ι profile is shown in Fig. 7(b). After less than 100 iterations, a minimum is achieved. The corresponding normalized cost function is $J = 0.0285$. Fig. 7(b) shows the ι profile achieved at some $T \in [T_1, T_2]$ that best matches the desirable ι profile. The corresponding time evolutions for the three actuators are shown in Fig. 8.

We now change the initial poloidal flux profile while keeping the same open-loop controller shown in Fig. 8. Fig. 7(a) shows the disturbed initial poloidal flux profile considered in this case, and compares it with the nominal initial poloidal flux profile. In this case, the cost function results $J = 0.0404$. Fig. 7(b) shows the difference between the obtained ι profile and the desirable ι profile. As expected, the matching is worsen due to the disturbance in the initial poloidal flux profile.

5.2 Closed-loop control (disturbance rejection)

In the third simulation case, we implement the closed-loop, receding-horizon control using the extremum seeking optimal control algorithm. At each sampling time $t_i = i \times 0.1s$ for $i = 1, \ldots, 11$, the actuator trajectories are updated using the solution to the stated optimal control problem provided by the extremum seeking control algorithm. At $t = t_0 = 0$, the "measured" ψ profile is the disturbed initial poloidal flux profile, shown in Fig. 7(a), and the open-loop actuator trajectories are used for control during the first time interval. After $\Delta t = 0.1s$, the control input is updated with the extremum seeking optimal result. The procedure is repeated until $t = T_1 = 1.2s$. From that instant the control input is kept unmodified until the end of the considered time interval at $T_2 = 2.4$. For each extremum seeking optimization at $t_i = i \times 0.1s$ for $i = 0, \ldots, 10$, the ψ profile is measured and incorporated into the control design procedure.

For the closed-loop controller, the achieved matching shown in Fig. 7(b) gives a cost function $J = 0.02510$. Fig. 9 shows the closed-loop control actuator trajectories. Fig. 7(b) compares the matching of the target ι for open-loop and closed-loop control. The closed-loop approach provides a better matching as it is illustrated by the results in Table 2.

Table 2. Comparison of open-loop and closed-loop control results.

	Cost function		
	off-line	open-loop	closed-loop
J	0.0285	0.0404	0.02510

6. CONCLUSIONS AND FUTURE WORK

A simplified dynamic model describing the evolution of the poloidal flux, and therefore the ι profile, during the inductive phase of the discharge has been introduced. Using this model, a closed-loop, multi-parameter extremum-seeking, receding-horizon, optimal controller has been proposed, and successfully tested in simulations, to match a desired ι profile within a predefined time window during the flattop phase of the tokamak discharge. The extremum-seeking procedure has shown to be effective in dealing with an optimal control problem defined for a nonlinear PDE system subject to many constraints in its actuators, and where not only interior and boundary control but also diffusivity control are considered. The proposed controller satisfactorily rejects disturbances in the initial poloidal flux profile.

The computational effort required by the proposed method may make real-time implementation challenging in short-discharge tokamaks. In order to overcome this limitation and reduce the computational burden, model reduction will be considered in future work. In addition, other nonlinear programming optimization techniques that may reduce the convergence time will also be considered.

REFERENCES

K. Ariyur and M. Krstic. *Real-Time Optimization by Extremum Seeking Feedback*. Wiley, 2003.

J.R. Ferron et al. Feedback control of the safety factor profile evolution during formation of an advanced tokamak discharge. *Nuclear Fusion*, 46(10):L13, 2006.

F.L. Hinton and R.D. Hazeltine. Theory of plasma transport in toroidal confinement systems. *Reviews of Modern Physics*, 48(2):239–308, 1976.

K. Ariyur J. Choi, M. Kristic and J. Lee. Extremum seeking control for discrete-time systems. *IEEE Transactions on Automatic Control*, 47(2):318–323, 2002.

L. Laborde et al. Towards fully non-inductive current drive operation in JET. *Plasma Physics and Controlled Fusion*, 47(1):155–183, 2005.

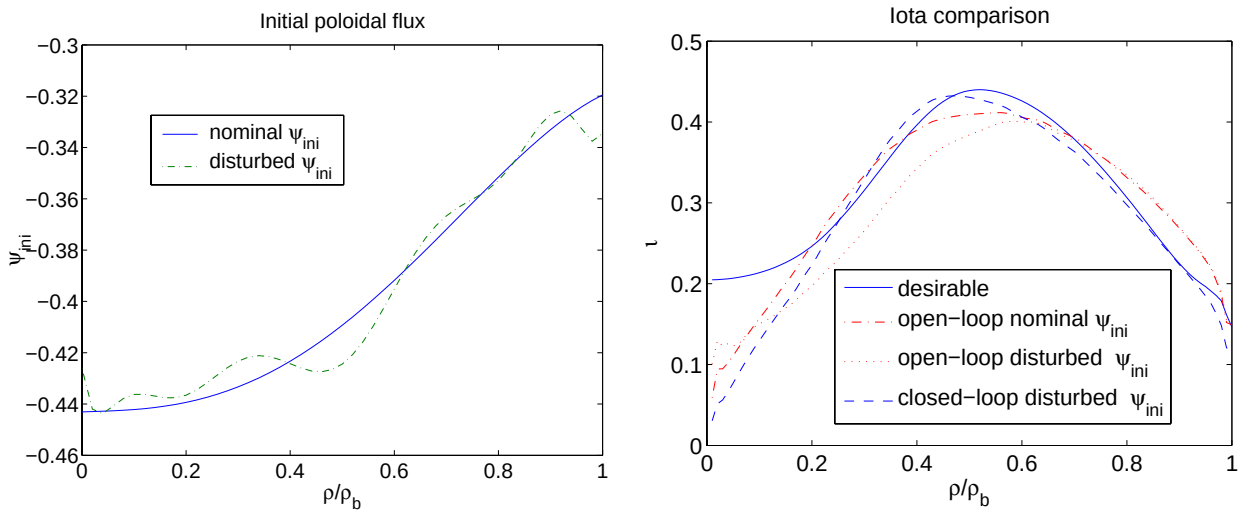

Fig. 7. Matching comparison: (a) nominal and perturbed initial flux profiles, (b) achieved ι profiles (best matching).

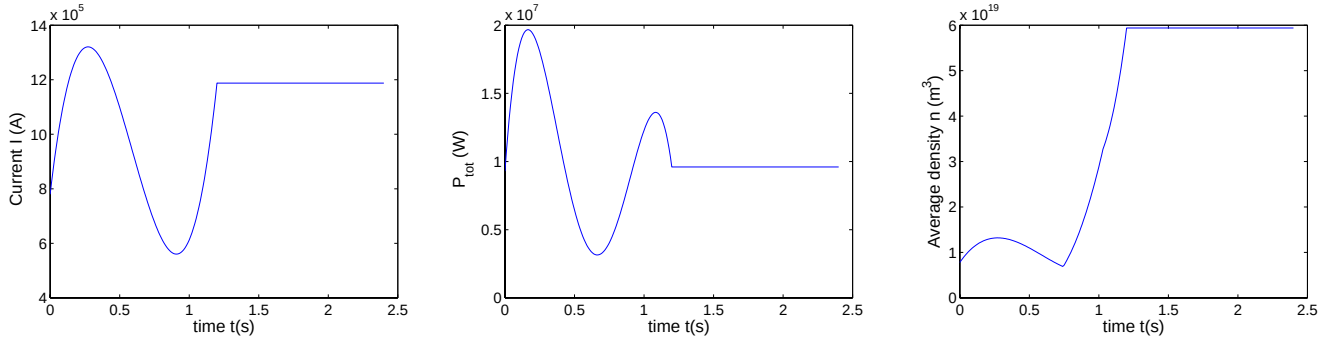

Fig. 8. Open-loop, extremum-seeking, optimal control: (a) $I(t)$, (b) P_{tot}, (c) $\bar{n}(t)$.

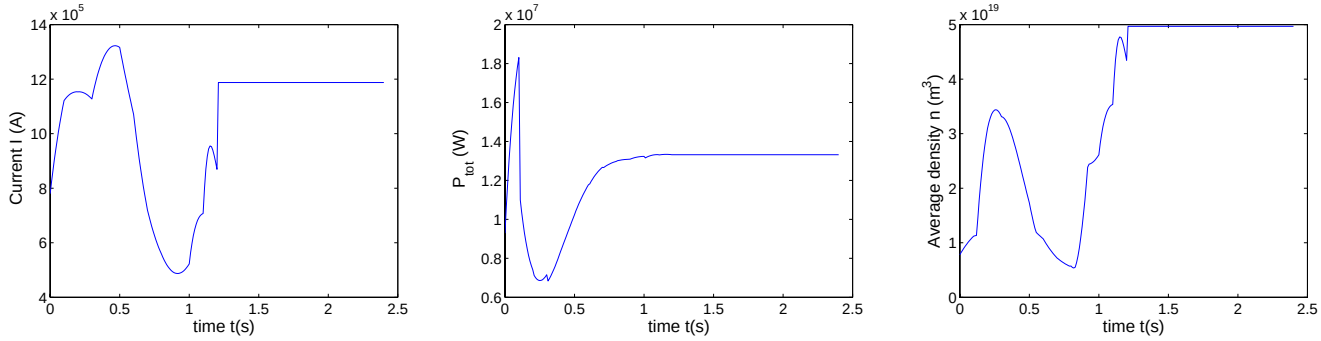

Fig. 9. Closed-loop, extremum-seeking, receding-horizon optimal control: (a) $I(t)$, (b) P_{tot}, (c) $\bar{n}(t)$.

D. Moreau et al. Real-time control of the q-profile in JET for steady state advanced tokamak operation. *Nuclear Fusion*, 43(9):870–82, 2003.

M. Murakami et al. Progress toward fully noninductive, high beta conditions in DIII-D. *Physics of Plasmas*, 13(5): 056106(1)–056106(9), 2006.

Y. Ou, E. Schuster, T. Luce, J. Ferron, M.L. Walker, and D.A. Humphreys. Towards model-based current profile control at DIII-D. *Fusion Engineering and Design*, 82:1153–1160, 2006.

A. Pironti and M. Walker. Fusion, tokamaks, and plasma control. *IEEE Control System Magazine*, 25(5):30–43, 2005.

E. Schuster and M. Ariola. The Role of Controls in Nuclear Fusion. In *Proceedings of the 45th IEEE Conference on Decision and Control*, 2006.

T. Suzuki et al. Recent RF experiments and application of RF waves to real-time control of safety factor profile in JT-60U. In *AIP Conference*, volume n 787, pages 279–86, 2005.

M.L. Walker, D.A. Humphreys, D. Moreau D. Mazon, M. Okabayashi, T.H. Osborne, and E. Schuster. Emerging applications in tokamak plasma control. Control solutions for next-generation tokamaks. *IEEE Control System Magazine*, 26(2): 35–63, April 2006.

T. Wijnands et al. Feedback control of the current profile on Tore Supra. *Nuclear Fusion*, 37(6):777, 1997.